Higher-Order Weyl Semimetals

Hai-Xiao Wang [1,2,3,4] Zhi-Kang Lin,[1] Bin Jiang,[1] Guang-Yu Guo,[3,4] and Jian-Hua Jiang [1,*]

[1]*School of Physical Science and Technology, and Collaborative Innovation Center of Suzhou Nano Science and Technology, Soochow University, 1 Shizi Street, Suzhou 215006, China*
[2]*School of Physical Science and Technology, Guangxi Normal University, Guilin 541004, China*
[3]*Department of Physics and Center for Theoretical Physics, National Taiwan University, Taipei 10617, Taiwan*
[4]*Physics Division, National Center for Theoretical Sciences, Hsinchu 30013, Taiwan*

Higher-order topology yields intriguing multidimensional topological phenomena, while Weyl semimetals have unconventional properties such as chiral anomaly. However, so far, Weyl physics remain disconnected with higher-order topology. Here, we report the theoretical discovery of higher-order Weyl semimetals and thereby the establishment of such an important connection. We demonstrate that higher-order Weyl semimetals can emerge in chiral materials such as chiral tetragonal crystals as the intermediate phase between the conventional Weyl semimetal and 3D higher-order topological phases. Higher-order Weyl semimetals manifest themselves uniquely by exhibiting concurrent chiral Fermi-arc surface states, topological hinge states, and the momentum-dependent fractional hinge charge, revealing a novel class of higher-order topological phases.

Introduction.—Topological insulators and semimetals with bulk-edge correspondence have invoked paradigm shifts in the study of condensed matter physics [1,2], photonics [3], acoustics [4,5], and phononics [6]. Recent discovery of higher-order topological insulators (HOTIs) [7–36], which exhibit gapped edge states and topologically protected corner and hinge states, unveils a new horizon beyond the conventional bulk-edge correspondence. The underlying bulk-edge-corner or bulk-surface-hinge correspondence manifests concurrent multidimensional topological physics, which is the most salient feature of higher-order topology. On the other hand, Weyl semimetals have been one of the focuses in the study of topological physics and materials, due to their anomalous physical properties (e.g., chiral anomaly) and their connection with various topological phases [e.g., three-dimensional (3D) quantum Hall effects] [37–47]. Although higher-order Dirac semimetals [48–51] have been proposed, Weyl semimetals, however, remain disconnected with higher-order topology.

In this Letter, we establish such a missing connection. The basic picture is illustrated in Fig. 1. If a 3D system is regarded as k_z-dependent two-dimensional (2D) systems, conventional Weyl points separate the 3D Brillouin zone into regions with quantum anomalous Hall insulator (QAHI) and normal insulator (NI) phases [Fig. 1(a)] [38,40,44,45]. In contrast, higher-order Weyl points (HOWPs) separate the 3D Brillouin zone into regions with QAHI and HOTI phases [Fig. 1(b)]. As a consequence, when measuring the hinge local density of states (LDOS), conventional Weyl semimetals exhibit only spectral features of topological surface states [Fig. 1(c)] [38,41,42,

44–46]. In comparison, the higher-order Weyl semimetals exhibit both spectral features of the surface states and the
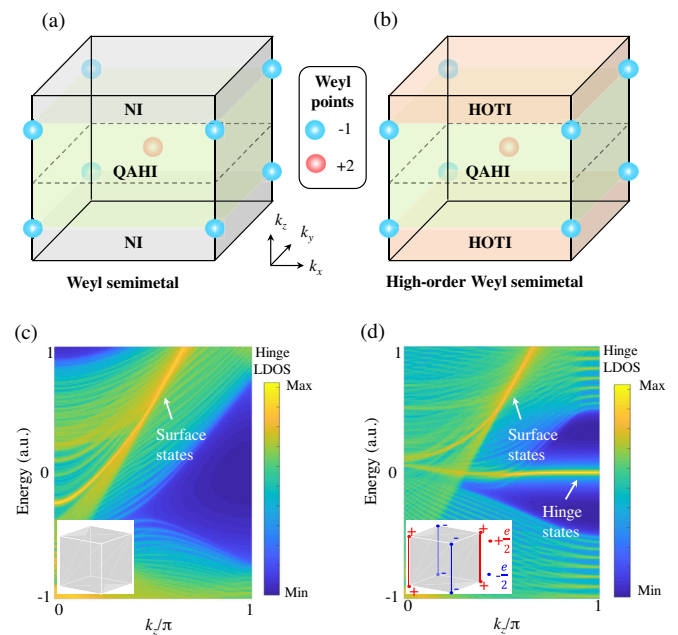

FIG. 1. Schematic of (a) conventional and (b) higher-order Weyl semimetals. Weyl points and their topological charges are depicted in the middle. Hinge LDOS for (c) conventional and (d) higher-order Weyl semimetals. Higher-order Weyl semimetal exhibits concurrent hinge and surface states and fractional hinge charges (see insets) in finite systems. Finite structures with 20×20 unit cells in the *x*-*y* plane are adopted in the calculation using models in Fig. 2.

higher-order hinge states [Fig. 1(d)]. In addition, due to the higher-order topology, fractional charge can emerge on the hinges of higher-order Weyl semimetals. The concurrent chiral Fermi-arc surface states, topological hinge states, and the momentum-dependent fractional hinge charge emerge as the hallmark characteristics of higher-order Weyl semi-metals. In comparison, higher-order Dirac semimetals have only topological hinge properties, since the higher-order Dirac points separate in **k**-space higher-order topological band gaps and trivial band gaps.

Model for the HOWPs.—To realize the HOWPs depicted in Fig. 1, we first notice that both QAHIs and quadrupole topological insulators (QTIs) can be realized using synthetic gauge fluxes [13,18,38,40,52]. QAHI is a "first-order" 2D topological insulator with quantized Hall conductance and chiral edge states [52]. In comparison, QTI is a "second-order" 2D topological insulator that hosts gapped edge states, topological corner states, and fractional corner charge $\pm 1/2$ with a quadrupole configuration [7,8]. We propose a tight-binding model with square-spiral structures, where translation along the z direction generates synthetic fluxes straightforwardly.

The tight-binding model based on tetragonal lattices is depicted in Fig. 2(a). For simplicity, the lattice constants along the x, y, z directions are set to unity. In each unit cell, there are four identical sites (indicated by the black spheres) arranged in the geometry as illustrated in Fig. 2. The structure exhibits square spirals as going from $1 \rightarrow 3 \rightarrow 2 \rightarrow 4$, yielding a fourfold screw symmetry $S_{4z} := (x, y, z) \rightarrow (y, -x, z + \frac{1}{4})$. In addition, there are two-fold rotation symmetries $C_{2x} := (x, y, z) \rightarrow (x, -y, -z)$ and $C_{2y} := (x, y, z) \rightarrow (-x, y, -z - \frac{1}{2})$, which, together with the time-reversal symmetry, protect the quadrupole topology.

The tight-binding Hamiltonian is given by

$$H = \sum_{\langle i,j \rangle} t_{\mathrm{NN}}(c_i^\dagger a_j + d_i^\dagger b_j + c_i^\dagger b_j + a_i^\dagger d_j)$$
$$+ \sum_{\langle\langle i,j \rangle\rangle} t_{\mathrm{NNN}}(a_i^\dagger b_j + c_i^\dagger d_j) + \mathrm{H.c.}, \quad (1)$$

where $a(a^\dagger)$, $b(b^\dagger)$, $c(c^\dagger)$, and $d(d^\dagger)$ are the annihilation (creation) operators on the sites 1–4, separately. At the right side of the equation, the first term describes the nearest-neighbor couplings, where $t_{\mathrm{NN}} = \gamma$ (λ) for the intracell (intercell) coupling. The second term denotes the next-nearest-neighbor couplings, where $t_{\mathrm{NNN}} = t_1$ (t_2) for the intracell (intercell) coupling. Their values are specified in the figure captions.

A top-down view is shown in Fig. 2(b), where the spiral directions are labeled by the arrows for different regions. The spiral structures introduce synthetic gauge fluxes $\pm\phi$ into these regions. Remarkably, such synthetic gauge fluxes are merely due to the translation along the z direction, which can be understood as follows: The site 4 in a unit cell
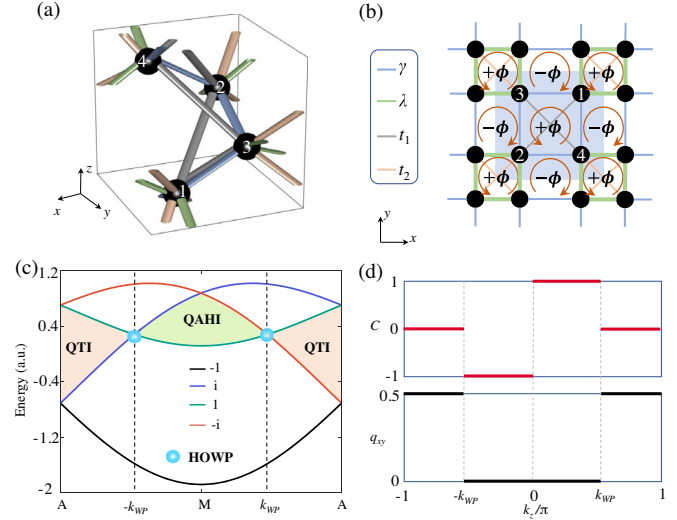

FIG. 2. (a) 3D tight-binding model with chiral couplings in tetragonal lattices. (b) Top-down view of the model. Brown arrows represent the spiral hopping structures that induce the synthetic gauge fluxes $\pm\phi$. (c) Evolution of energy bands and $\tilde{C}_{4z}$ eigenvalues along the $A - M - A$ line. The gap between the second and third bands experiences topological transitions from QTI to QAHI via the HOWPs. (d) Evolution of Chern number $\mathcal{C}$ (upper) and quadrupole index q_{xy} (lower) with k_z for the gap between the second and third bands. Parameters for higher-order Weyl phase: $\gamma = 0.6$, $\lambda = 1$, $t_1 = 0.2$, and $t_2 = 0.24$. The conventional Weyl phase in Fig. 1 is realized by the following exchanges: $\lambda \leftrightarrow \gamma$, $t_1 \leftrightarrow t_2$.

of central coordinate (X, Y, Z) couples only to the site 1 in the upper unit cell of central coordinate $(X, Y, Z + 1)$. Such a coupling naturally picks up a translational phase $\phi = k_z$. We remark that our model, with time-reversal symmetry and using only positive couplings, is more feasible than other models for quadrupole topology, where either a mixture of positive and negative couplings or magnetic fluxes are required [7,17,48].

The synthetic gauge fluxes are crucial in our construc-tion. First, they give rise to the emergence of the QAHIs with Chern number $\mathcal{C} = 1$ (-1) for $0 < k_z < k_{\mathrm{WP}}$ ($-k_{\mathrm{WP}} < k_z < 0$). Second, they yield the QTI phase with a quadrupole index $q_{xy} = \frac{1}{2}$ for $|k_z| > k_{\mathrm{WP}}$ (see Supplemental Material for the characterizations of these two topological phases [53]). Here, the HOWPs appear at the wave vectors $(\pi, \pi, \pm k_{\mathrm{WP}})$ with a topological charge of -1. According to the Nielsen-Ninomiya theorem [61], to compensate the nonzero total charge of these HOWPs [61], a quadratic Weyl point with charge $+2$ appears at the Γ point. If the 3D system is viewed as k_z-dependent 2D systems, the HOWPs can then be regarded as the transitions between the QAHIs and QTIs.

The Chern number and the quadrupole index can be determined through two approaches. First, straightforward calculations based on the Wilson-loop and nested Wilson-loop approaches confirm the above picture (see

Supplemental Material for details [53]). The eigenvalues of the (nested) Wilson-loop operator gives the (nested) Wannier bands. The region with $|k_z| < |k_{WP}|$ exhibits gapless Wannier bands, of which the winding property gives the Chern numbers shown in Fig. 2(d). The change of the Chern number $\mathcal{C}$ at $k_z = 0$ is due to the quadratic Weyl point at the Γ point, while the change at $k_z = \pm k_{WP}$ is due to the HOWPs. In comparison, the region with $|k_z| > |k_{WP}|$ exhibits gapped Wannier bands. The nested Wannier bands yield quantized Wannier band polarizations and nontrivial quadrupole index $q_{xy} = \frac{1}{2}$ (see Supplemental Material for details [53]). The quantization of the Wannier band polarizations and the quadrupole index to zero or $\frac{1}{2}$ are dictated by the symmetry operators $\Theta_x = C_{2x}\mathcal{T}$ and $\Theta_y = C_{2y}\mathcal{T}$, where $\mathcal{T}$ is the time-reversal operator (see proof in the Supplemental Material [53]). The noncommutativeness of the Θ_x and Θ_y operators are crucial for the emergence of the gapped Wannier bands [8]. Though the synthetic flux model is quite different from the original model for quadrupole topological insulators proposed in Ref. [7], it does support a quadrupole topological band gap with different protective symmetries, as validated in details in the Supplemental Material [53].

On the other hand, the quadrupole index can be extracted from the rotation eigenvalues at the high-symmetry points [8,20]. Specifically, for each k_z, we examine the eigenvalues of the pseudorotation operator $\tilde{C}_{4z} = e^{-ik_z/4}S_{4z}$ at the $\tilde{\Gamma} = (0, 0, k_z)$ and $\tilde{M} = (\pi, \pi, k_z)$ points. The first band always has $\tilde{C}_{4z}(\tilde{\Gamma}) = 1$, while the second band has $\tilde{C}_{4z}(\tilde{\Gamma}) = i$ $(-i)$ for $k_z > 0$ $(k_z < 0)$. In comparison, the rotation eigenvalues at the $\tilde{M}$ point vary with k_z, as presented in Fig. 2(c). The quadrupole index is related to the rotation eigenvalues as [8,20]

$$\exp(i2\pi q_{xy}) = r_4^-(\tilde{\Gamma})r_4^-(\tilde{M})^*. \qquad (2)$$

Here, r_4^- denotes the $\tilde{C}_{4z}$ eigenvalues of $\pm i$. From the $\tilde{C}_{4z}$ eigenvalues in Fig. 2(c), one obtains quadrupole topological numbers consistent with those in Fig. 2(d). The band inversion between the second and third bands along the A-M-A line triggers the transition between the QAHI phases and the QTI phase, and thus leads to the formation of the HOWPs.

Topological surface states.—The coexistence of the conventional and higher-order topology is manifested in the topological surface states. Depending on the wave vector k_z, the topological surface states can be gapless or gapped. As shown in Fig. 3(a), the surface states are gapless along the $\bar{\Gamma}\bar{Y}$ line, while the surface states become gapped along the $\bar{R}\bar{Z}$ line. The former originates from the gapless chiral edge states in the QAHI phases, while the latter results from the gapped edge states in the QTI phase.

We further study the topological surface states by examining the surface LDOS at given energies. We sample
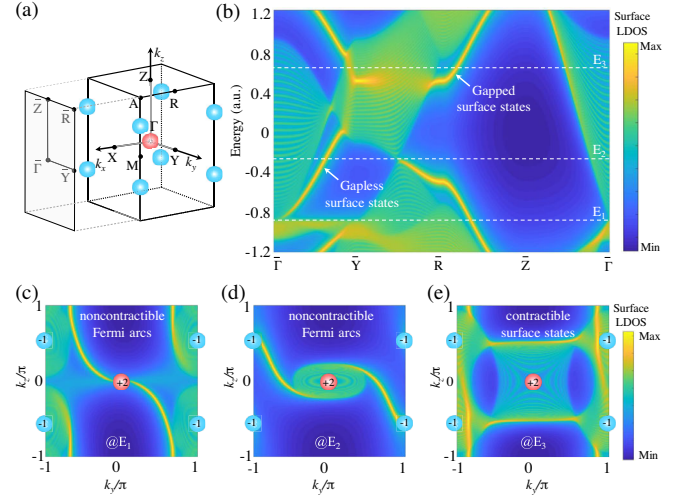

FIG. 3. (a) Bulk and (100) surface Brillouin zones. (b) Surface LDOS for the (100) surface along high-symmetry lines. (c)–(e) Surface LDOS at three different energies labeled in (b) as dashed lines. $E_1 = -0.85$ ($E_2 = -0.27$) is at the energy of the quadratic Weyl points (the HOWPs), while $E_3 = 0.6$. Parameters are the same as in Fig. 2.

three different energies: E_1 is exactly at the energy of the quadratic Weyl points, E_2 is exactly at the energy of the HOWPs, and E_3 is an energy above. At E_1 and E_2, there are Fermi-arc surface states connecting the projection of the quadratic Weyl point at $\bar{\Gamma}$ and the projections of the HOWPs at the surface Brillouin zone boundary. These chiral Fermi arcs connecting projections of Weyl points with opposite charges are consistent with the conventional picture [42]. Nevertheless, the isoenergy curves form noncontractible loops winding around the torus of the surface Brillouin zone, which is different from the short Fermi arcs observed in many electronic systems [47]. In comparison, at E_3, the contractible surface states emerging at large $|k_z|$, which do not connect Weyl points with opposite topological charges, originate from the gapped surface states due to the quadrupole topology.

Topological hinge states and fractional hinge charge.— We now turn to the manifestation of the higher-order topology at the hinges. First, taking $k_z = \pi$ as an example to illustrate the underlying physics, the bulk and surface spectra are depicted in Fig. 4(a), which shows clearly the gapped surface states within the bulk band gap. For a finite system with four hinges, the eigenspectrum exhibits four hinge states within the surface band gap whose wave functions are localized around the four hinges. The concurrent bulk, surface, and hinge states appearing for $|k_z| > k_{WP}$ [as shown in Fig. 1(d)] demonstrate straightforwardly the higher-order topology.

One of the remarkable properties of the QTI is the fractional corner charge [7,62] $\pm 1/2$, with a quadrupole configuration as depicted in the inset of Fig. 4(c). We calculate the hinge charge at half-filling through $Q_h = \sum_\alpha P_\alpha^{\text{hinge}}$

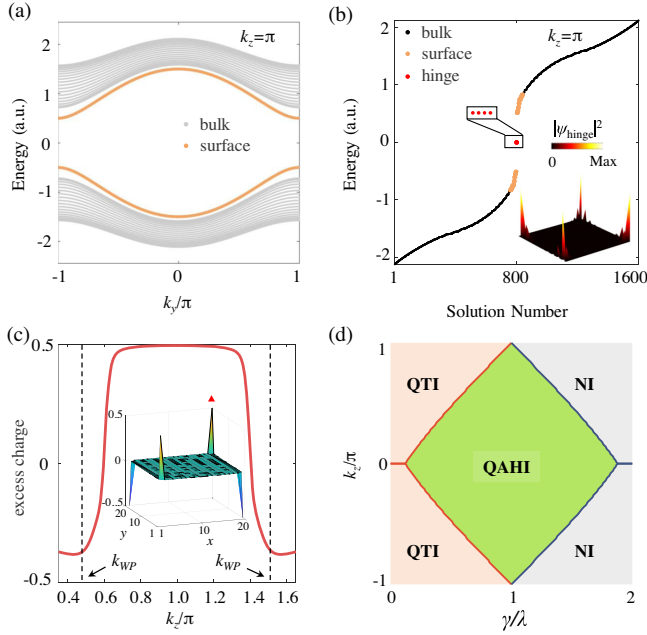FIG. 4. (a) Bulk and (100) surface spectra for $k_z = \pi$, showing gapped surface states. (b) Eigenspectrum for a finite-sized system with 20×20 unit cells in the $x - y$ plane for $k_z = \pi$, showing coexisting gapped bulk and surface states together with the fourfold degenerate hinge states. Inset shows the wave function of the hinge states. (c) Fractional hinge charge at the right-upper hinge (labeled by the red triangle in the inset) vs k_z calculated for a finite system with 20×20 unit cells in the $x - y$ plane. Inset shows the quadrupole configuration of the hinge charge. (d) Phase diagram of the system with $\lambda = 1$, $t_1 = 0.2$, and $t_2 = 0.24$.

where P_α^{hinge} is the probability of finding an electron in the hinge region for a filled state α. Using this method, we obtain the fractional hinge charge Q_h for various k_z by considering a hinge region with 4×4 unit cells in a finite system consisting of 20×20 unit cells in the $x - y$ plane (see Supplemental Material for details [53]). It is seen from Fig. 4(c) that the hinge charge gradually reaches the quantized fractional value of $1/2$ for $|k_z| > k_{\text{WP}}$. The crossover behavior around the Weyl point is due to the finite-size effects.

Phase diagram.—Finally, we study the phase diagram when the intracell nearest-neighbor coupling γ is varied. In Fig. 4(d), we present the evolution of the Weyl points along the *A-M-A* line with the parameter γ. It is seen that, for $\gamma < \lambda$, the system is a higher-order Weyl semimetal. k_{WP} decreases with decreasing γ. In the regime $\gamma < 0.12\lambda$, we find that $k_{\text{WP}} \to 0$ and the system becomes a 3D quadrupole topological phase. In comparison, the system is a conventional Weyl semimetal when $\gamma > \lambda$. Therefore, the higher-order Weyl semimetal phase emerges as the intermediate phase between the conventional Weyl semimetal and 3D quadrupole topological phases. On the other hand, by regarding the 3D system as k_z-dependent 2D systems, the HOWPs serve as the boundary between the QAHI phases and the QTI phase, whereas the conventional Weyl

points serve as the boundary between the QAHI phases and the NI phase.

Conclusion and outlook.—In this Letter, we unveil the concept of HOWPs as a type of Weyl points connected with higher-order topology. When the 3D system is regarded as k_z-dependent 2D systems, HOWPs appear as the transition points between the QAHIs and the HOTI with quadrupole topology. Experimental signatures of the higher-order Weyl points consist of the coexistence of Fermi-arc surface states and the topological hinge states, as well as the k_z-dependent fractional charge at the hinges. The HOWPs can be realized in tetragonal chiral crystals with the S_{4z}, C_{2x}, C_{2y}, and $\mathcal{T}$ symmetries. Potential material candidates in electronic and acoustic systems are suggested in the Supplemental Material [53]. We remark that, due to the richness of HOTIs, there are many other types of HOWPs where the HOTI phase can be realized without the quadrupole topology (e.g., HOTI phases with quantized Wannier centers [62]). The study of higher-order topological degeneracies thus opens a frontier in topological physics.

Note added.—Recently, we noticed two preprints appeared [63,64] in parallel with our work on higher-order Weyl semimetals.

---

[*]jianhuajiang@suda.edu.cn

[1] M. Z. Hasan and C. L. Kane, Colloquium: Topological insulators, Rev. Mod. Phys. **82**, 3045 (2010).

[2] X.-L. Qi and S.-C. Zhang, Topological insulators and superconductors, Rev. Mod. Phys. **83**, 1057 (2011).

[3] T. Ozawa *et al.*, Topological photonics, Rev. Mod. Phys. **91**, 015006 (2019).

[4] G. Ma, M. Xiao, and C. T. Chan, Topological phases in acoustic and mechanical systems, Nat. Rev. Phys. **1**, 281 (2019).

[5] X. Zhang, M. Xiao, Y. Cheng, M.-H. Lu, and J. Christensen, Topological sound, Commun. Phys. **1**, 97 (2018).

[6] Y. Liu, X. Chen, and Y. Xu, Topological phononics: From fundamental models to real materials, Adv. Funct. Mater. **30**, 1904784 (2020).

[7] W. A. Benalcazar, B. A. Bernevig, and T. L. Hughes, Quantized electric multipole insulators, Science **357**, 61 (2017).

[8] W. A. Benalcazar, B. A. Bernevig, and T. L. Hughes, Electric multipole moments, topological multipole moment pumping, and chiral hinge states in crystalline insulators, Phys. Rev. B **96**, 245115 (2017).

[9] J. Langbehn, Y. Peng, L. Trifunovic, F. v. Oppen, and P. W. Brouwer, Reflection-Symmetric Second-Order Topological

Insulators and Superconductors, Phys. Rev. Lett. **119,** 246401 (2017).

[10] Z. Song, Z. Fang, and C. Fang, $(d-2)$-Dimensional Edge States of Rotation Symmetry Protected Topological States, Phys. Rev. Lett. **119,** 246402 (2017).

[11] F. Schindler, A. M. Cook, M. G. Vergniory, Z. Wang, S. S. P. Parkin, B. A. Bernevig, and T. Neupert, Higher-order topological insulators, Sci. Adv. **4,** eaat0346 (2018).

[12] M. Serra-Garcia, V. Peri, R. Susstrunk, O. R. Bilal, T. Larsen, L. G. Villanueva, and S. D. Huber, Observation of a phononic quadrupole topological insulator, Nature (London) **555,** 342 (2018).

[13] C. W. Peterson, W. A. Benalcazar, T. L. Hughes, and G. Bahl, A quantized microwave quadrupole insulator with topologically protected corner states, Nature (London) **555,** 346 (2018).

[14] S. Imhof *et al.*, Topolectrical-circuit realization of topological corner modes, Nat. Phys. **14,** 925 (2018).

[15] J. Noh, W. A. Benalcazar, S. Huang, M. J. Collins, K. P. Chen, T. L. Hughes, and M. C. Rechtsman, Topological protection of photonic mid-gap defect modes, Nat. Photonics **12,** 408 (2018).

[16] M. Ezawa, Higher-Order Topological Insulators and Semimetals on the Breathing Kagome and Pyrochlore Lattices, Phys. Rev. Lett. **120,** 026801 (2018).

[17] S. Franca, J. van den Brink, and I. C. Fulga, An anomalous higher-order topological insulator, Phys. Rev. B **98,** 201114 (R) (2018).

[18] S. Mittal, V. V. Orre, G. Zhu, M. A. Gorlach, A. Poddubny, and M. Hafezi, Photonic quadrupole topological phases, Nat. Photonics **13,** 692 (2019).

[19] B. J. Wieder, Z. Wang, J. Cano, X. Dai, L. M. Schoop, B. Bradlyn, and B. A. Bernevig, Strong and fragile topological Dirac semimetals with higher-order Fermi arcs, Nat. Commun. **11,** 627 (2020).

[20] L. He, Z. Addison, E. J. Mele, and B. Zhen, Quadrupole topological photonic crystals, Nat. Commun. **11,** 3119 (2020).

[21] Q.-B. Zeng, Y.-B. Yang, and Y. Xu, Higher-order topological insulators and semimetals in generalized Aubry-Andr-Harper models, Phys. Rev. B **101,** 241104(R) (2020).

[22] X. Zhang, Z.-K. Lin, H.-X. Wang, Z. Xiong, Y. Tian, M.-H. Lu, Y.-F. Chen, and J.-H. Jiang, Symmetry-protected hierarchy of anomalous multipole topological band gaps in nonsymmorphic metacrystals, Nat. Commun. **11,** 65 (2020).

[23] Y. Chen, Z.-K. Lin, H. Chen, and J.-H. Jiang, Plasmon-polaritonic quadrupole topological insulators, Phys. Rev. B **101,** 041109(R) (2020).

[24] Y. Qi, C. Qiu, M. Xiao, H. He, M. Ke, and Z. Liu, Acoustic Realization of Quadrupole Topological Insulators, Phys. Rev. Lett. **124,** 206601 (2020).

[25] B.-Y. Xie, H.-F. Wang, H.-X. Wang, X.-Y. Zhu, J.-H. Jiang, M.-H. Lu, and Y.-F. Chen, Second-order photonic topological insulator with corner states, Phys. Rev. B **98,** 205147 (2018).

[26] H. Xue, Y. Yang, F. Gao, Y. Chong, and B. Zhang, Acoustic higher-order topological insulator on a kagome lattice, Nat. Mater. **18,** 108 (2019).

[27] X. Ni, M. Weiner, A. Alu, and A. B. Khanikaev, Observation of higher-order topological acoustic states protected by generalized chiral symmetry, Nat. Mater. **18,** 113 (2019).

[28] X. Zhang, H.-X. Wang, Z.-K. Lin, Y. Tian, B. Xie, M.-H. Lu, Y.-F. Chen, and J.-H. Jiang, Second-order topology and multidimensional topological transitions in sonic crystals, Nat. Phys. **15,** 582 (2019).

[29] A. E. Hassan, F. K. Kunst, A. Moritz, G. Andler, E. J. Bergholtz, and M. Bourennane, Corner states of light in photonic waveguides, Nat. Photonics **13,** 697 (2019).

[30] S. Liu, W. Gao, Q. Zhang, S. Ma, L. Zhang, C. Liu, Y. J. Xiang, T. J. Cui, and S. Zhang, Topologically protected edge state in two-dimensional Su-Schrieffer-Heeger circuit, Research **2019,** 8609875 (2019).

[31] Y. Ota, F. Liu, R. Katsumi, K. Watanabe, K. Wakabayashi, Y. Arakawa, and S. Iwamoto, Photonic crystal nanocavity based on a topological corner state, Optica **6,** 786 (2019).

[32] Z. Zhang, H. Long, C. Liu, C. Shao, Y. Cheng, X. Liu, and J. Christensen, Deep subwavelength holey acoustic second order topological insulators, Adv. Mater. **31,** 1904682 (2019).

[33] H. Fan, B. Xia, L. Tong, S. Zheng, and D. Yu, Elastic Higher-Order Topological Insulator with Topologically Protected Corner States, Phys. Rev. Lett. **122,** 204301 (2019).

[34] X.-D. Chen, W.-M. Deng, F.-L. Shi, F.-L. Zhao, M. Chen, and J.-W. Dong, Direct Observation of Corner States in Second-Order Topological Photonic Crystal Slabs, Phys. Rev. Lett. **122,** 233902 (2019).

[35] B.-Y. Xie, G.-X. Su, H.-F. Wang, H. Su, X.-P. Shen, P. Zhan, M.-H. Lu, Z.-L. Wang, and Y.-F. Chen, Visualization of Higher-Order Topological Insulating Phases in Two-Dimensional Dielectric Photonic Crystals, Phys. Rev. Lett. **122,** 233903 (2019).

[36] L. Zhang, Y. Yang, P. Qin, Q. Chen, F. Gao, E. Li, J.-H. Jiang, B. Zhang, and H. Chen, Higher order topological states in surface wave photonic crystals, Adv. Sci. **7,** 1902724 (2020).

[37] X. Wan, A. M. Turner, A. Vishwanath, and S. Y. Savrasov, Topological semimetal and Fermi-arc surface states in the electronic structure of pyrochlore iridates, Phys. Rev. B **83,** 205101 (2011).

[38] J.-H. Jiang, Tunable topological Weyl semimetal from simple-cubic lattices with staggered fluxes, Phys. Rev. A **85,** 033640 (2012).

[39] L. Lu, L. Fu, J. D. Joannopoulos, and M. Soljai, Weyl points and line nodes in gyroid photonic crystals, Nat. Photonics **7,** 294 (2013).

[40] M. Xiao, W.-J. Chen, W.-Y. He, and C. T. Chan, Geometric phase and band inversion in periodic acoustic systems, Nat. Phys. **11,** 240 (2015).

[41] L. Lu, Z. Wang, D. Ye, L. Ran, L. Fu, J. D. Joannopoulos, and M. Soljai, Experimental observation of Weyl points, Science **349,** 622 (2015).

[42] C. Fang, L. Lu, and L. Fu, Topological semimetals with helicoid surface states, Nat. Phys. **12,** 936 (2016).

[43] B. Yan and C. Felser, Topological materials: Weyl semimetals, Annu. Rev. Condens. Matter Phys. **8,** 337 (2017).

[44] F. Li, X. Huang, J. Lu, J. Ma, and Z. Liu, Weyl points and Fermi arcs in a chiral phononic crystal, Nat. Phys. **14**, 30 (2018).

[45] H. Ge, X. Ni, T. Tian, S. Gupta, M.-H. Lu, X. Lin, W.-D. Huang, C. T. Chan, and Y.-F. Chen, Experimental Observation of Acoustic Weyl Points and Topological Surface States, Phys. Rev. Applied **10**, 014017 (2018).

[46] B. Yang *et al.*, Ideal Weyl points and helicoid surface states in artificial photonic crystal structures, Science **359**, 1013 (2018).

[47] N. P. Armitage, E. J. Mele, and A. Vishwanath, Weyl and Dirac semimetals in three-dimensional solids, Rev. Mod. Phys. **90**, 015001 (2018).

[48] M. Lin and T. L. Hughes, Topological quadrupolar semimetals, Phys. Rev. B **98**, 241103(R) (2018).

[49] B. J. Wieder, Z. Wang, J. Cano, X. Dai, L. M. Schoop, B. Bradlyn, and B. A. Bernevig, Strong and fragile topological Dirac semimetals with higher-order Fermi arcs, Nat. Commun. **11**, 627 (2020).

[50] W. Wu, Z.-M. Yu, X. Zhou, Y. X. Zhao, and S. A. Yang, Higher-order Dirac fermions in three dimensions, Phys. Rev. B **101**, 205134 (2020).

[51] B. Roy, Higher-order topological superconductors in $\mathcal{P}$-, $\mathcal{T}$-odd quadrupolar Dirac materials, Phys. Rev. B **101**, 220506 (R) (2020).

[52] F. D. M. Haldane, Model for a Quantum Hall Effect without Landau Levels: Condensed-Matter Realization of the "Parity Anomaly", Phys. Rev. Lett. **61**, 2015 (1988).

[53] See Supplemental Material at http://link.aps.org/supplemental/10.1103/PhysRevLett.125.146401 for details on (I) the calculation of Wannier bands using the Wilson-loop approach, (II) the calculation of the quadrupole index, (III) symmetry constraints and the quantization of Wannier band polarizations and the quadrupole index, (IV) the calculation of the fractional hinge charge, (V) the calculation of the surface and hinge LDOS, and (VI) the potential material candidates in electronic and acoustic systems, which includes Refs. [54–60].

[54] *Inorganic Crystal Structure Database (ICSD)* (Fachinformationszentrum Karlsruhe, Karlsruhe, Germany, 2015).

[55] Bilbao Crystallographic Server, http://www.cryst.ehu.es.

[56] R. Pottgen, V. Hlukhyy, A. Baranov, and Y. Grin, Crystal structure and chemical bonding of Mg_3Ru_2, Inorg. Chem. **47**, 6051 (2008).

[57] P. Gressier, A. Meerschaut, L. Guemas, J. Rouxel, and P. Monceau, Characterization of the new series of quasi one-dimensional compounds $(MX_4)_nY$ (M = Nb, Ta; X = S, Se; Y = Br, I), J. Solid State Chem. **51**, 141 (1984).

[58] W. Shi, B. J. Wieder, H. L. Meyerheim, Y. Sun, Y. Zhang, Y. Li, L. Shen, Y. Qi, L. Yang, J. Jena, P. Werner, K. Koepernik, S. Parkin, Y. Chen, C. Felser, B. A. Bernevig, and Z. Wang, A charge-density-wave Weyl semimetal, arXiv:1909.04037.

[59] G. E. Pringle, The structure of $SrSi_2$: A crystal of class O (432), Acta Crystallogr. Sect. B **28**, 2326 (1972).

[60] S. M. Huang, S.-Y. Xu, I. Belopolski, C.-C. Lee, G. Chang, T.-R. Chang, B. Wang, N. Alidoust, G. Bian, M. Neupane, D. Sanchez, H. Zheng, H.-T. Jeng, A. Bansil, T. Neupert, H. Lin, and M. Z. Hasan, New type of Weyl semimetal with quadratic double Weyl fermions, Proc. Natl. Acad. Sci. U.S.A. **113**, 1180 (2016).

[61] H. B. Nielsen and M. Ninomiya, A no-go theorem for regularizing chiral fermions, Phys. Lett. **105B**, 219 (1981).

[62] W. A. Beanalcazar, T. Li, and T. L. Hughes, Quantization of fractional corner charge in C_n-symmetric higher-order topological crystalline insulators, Phys. Rev. B **99**, 245151 (2019).

[63] S. A. A. Ghorashi, T. Li, and T. L. Hughes, Higher-order Weyl Semimetals, arXiv:2007.02956.

[64] Q. Wei, X. Zhang, W. Deng, J. Lu, X. Huang, M. Yan, G. Chen, Z. Liu, and S. Jia, Higher-order topological semimetal in phononic crystals, arXiv:2007.03935.